Materials Physics and Mechanics. 2022;50(1): 89-106
Research article
http://dx.doi.org/10.18149/MPM.5012022_7

Submitted: March 10, 2022
Approved: May 6, 2022
Accepted: September 15, 2022

Microstructural modeling and prediction of effective elastic properties in 3D reinforced composite material

A.N. Anoshkin, P.V. Pisarev, D.A. Ermakov, K.V. Roman✉

Perm National Research Polytechnic University, Perm, Russia

✉ kvroman@pstu.ru

Abstract: We consider a textile composite material reinforced by carbon fibers with 3D orthogonal braiding and a polymer matrix. Microstructural studies were carried out to find the mean values and variation coefficients for the parameters of the braid unit cell within the reinforcement cage. We have constructed an algorithm along with geometric models for cells and fragments of the composite structure, providing different descriptions for the parameters of the binder yarn. The micromechanics problem was solved by the local approximation method; the fields of structural stresses and strains were determined for different models of composite fragments. The fields were averaged to compute the composite's effective elastic properties compared to the experimental data.

Keywords: spatially reinforced composite material, microstructure, experimental studies, unit cell, mathematical modeling, micromechanics, local approximation method, effective elastic properties

Acknowledgments*. The study was financed by the Ministry of Science and Higher Education of the Russian Federation within the framework of the program of activities of the Scientific and Educational Center Rational Subsoil Use.*

Citation: Anoshkin AN, Pisarev PV, Ermakov DA, Roman KV. Microstructural modeling and prediction of effective elastic properties in 3D reinforced composite material. *Materials Physics and Mechanics*. 2022;50(1): 89-106. DOI: 10.18149/MPM.5012022_7.

1. Introduction

Developing 3D reinforced composites (3DRC) incorporating woven, interlock, or rod reinforcements is a promising direction for advancing structures and technologies of composite materials [1]. 3D composite materials with a diverse range of physical and mechanical properties can be produced by tailoring the braiding pattern or the number and type of fibers along the reinforcement directions. In particular, the tear strength in the transverse direction and the shear resistance can be considerably improved in comparison with layered composite materials.

Modern braiding technologies allow generating complex 3D reinforcement cages that can be further impregnated to manufacture preforms whose shapes closely match the required component, reducing the labor intensity and production costs [2]. Spatially reinforced composite materials are increasingly in demand in aerospace engineering for heavily loaded structures, with an ever-widening range of applications.

As more versatile tools emerge for configuring the braiding patterns, novel approaches are developed for predicting effective mechanical characteristics and selecting the optimal

parameters of 3DRC structures for specific components. This paper is dedicated to constructing geometric structural models and predicting the effective elastic characteristics of the 3D reinforced composite accounting for mechanical tolerances in the braiding pattern of the reinforcement cage.

Specialized software packages are used for constructing geometric models describing the 3DRC structure: the best-known examples include TexGen, WiseTex, and Techtext CAD [3-14]. TexGen is an open-source software package developed by the research team led by Prof. Long at the University of Nottingham in 2006 [3-5]. The software can generate unit cells for the braiding pattern, with the geometric parameters input via the menu interface (these include the number of warp and weft yarns, width, height, and spacing for each set of yarns, etc.). WiseTex is a software package developed by Lomov's research group at KU Leuven in 2000 [6–10], capable of not only modeling the geometric structure of cells and fragments of textile composites like TexGen but also predicting their effective elastic properties. Furthermore, WiseTex incorporates an algorithm coding structural topology, providing additional options for computer simulation of geometric models for complex braiding patterns in 3DRC. The TechText CAD software package was developed at the University of Manchester in 2000-2002. It allows modelling the geometric structure of interlock woven fabrics and their deformation during manufacture [11-14]. In addition, TechText CAD can compile additional modules for controlling the production of interlock preforms with industrial weaving machines based on the simulation results.

It should be borne in mind that the above software packages simulate 'idealized' woven textiles corresponding to a given reinforcement geometry within the materials. They can be used to extract qualitative estimates for the effective elastic characteristics of the material from the given parameters of the structure. However, the operational parameters of 3D reinforcements and composite materials based on them (tensile forces and thicknesses for different yarn sets, pressures and flow rates of the impregnating agent, etc.) can fluctuate wildly during manufacture. This inevitably produces deviations/variations in the geometric parameters of the cage, such as paths of yarns, areas, and shapes of their cross-sections, and spacings between the yarns. These fluctuations in the material structure vary in different areas of the component because the textile reinforcement is deformed unevenly throughout the manufacturing process. The effect of these fluctuations in the parameters of the reinforcement cage on the mechanical characteristics of 3DRC has received scarce attention this far. Therefore, it remains to be elucidated whether the software packages developed for modeling geometric structures are suitable for predicting the effective elastic characteristics of real composite materials. We intend to explore this issue in our study.

Efforts should be made to construct models of the real structure of 3D reinforced composites accounting for random or regular deviations in the operational parameters and to assess the effect of these deviations on the elastic characteristics of the composite material. This paper presents the estimates obtained from the results of tomographic and microstructural studies on the parameters of the geometric structure in 3DRC specimens. The resulting estimates were used to construct computational geometric models of the unit cell and fragments of the 3DRC structure with the help of the TexGen software package and an algorithm we developed, aimed at solving the micromechanics problem for 3DRC in fragments of the structure based on local approximation [15]. The algorithm was applied to numerically solve boundary-value problems and compute the effective elastic properties of 3D reinforced composite. The predicted effective elastic properties are compared with the results of mechanical tests in 3DRC specimens.

We intend to resolve the challenge of improving the prediction accuracy for the effective elastic properties in real 3D reinforced composites accounting for manufacturing tolerances in the structure parameters. Moreover, the newly available models can serve for

analyzing how the spread in geometric parameters of the composite structure affects its mechanical characteristics, predicting nonlinear deformation and strength estimates in 3DRC under complex loading.

2. 3D reinforced composite material

We consider a 3D reinforced textile composite with a repeating orthogonal braiding pattern. The preform of the analysed material is a plate with constant thickness, containing 10×10 to 15×15 repeating unit cells in a plane and one cell in the bulk of the plate. Thus, the spatial structure of the weave in the material can be assumed to be repeating in the plane and having a finite size in the third direction. The composite material is prepared by pressurized impregnation of a textile reinforcement cage with a polymer adhesive in a rigid mold.

The repeating cell of the tested material contains two rows of warp yarns, three rows of weft yarns, and two binder yarns (Fig. 1) [16]. The yarns are complex and contain approximately 12,000-15,000 elementary fibers (filaments) [16]. The filaments in the unit cell are characterized by their paths and can have different thicknesses, densities and cross-sectional shapes. Both single and double yarns can be used for cell braiding. Next, we consider a particular case of a unit cell where the weft centerline is a double yarn, and the remaining yarns are single. The mechanical behavior of the filaments in the 3DRC composite is generally described by models of fiber bundles or unidirectional fiber composites; the latter is adopted in this study. The model used is described in [17,18].

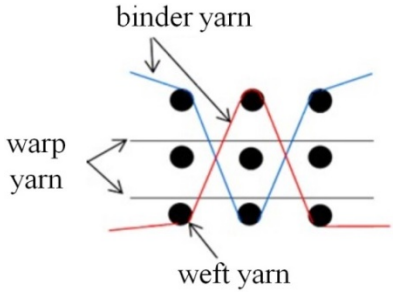

Fig. 1. Reinforcement scheme of repeating unit cell in 3DRC

The racetrack model, first introduced by Kemp [19], was used to describe the unit cell of the material considered in the paper (Fig. 2). The warp and weft yarns are taken to be straight in this model, while the binder yarn is represented by a line segment passing between the warp yarns and connected to two arcs passing around the weft yarns. This description of the binder yarn is simpler than the spline approximation used by other models, for example, in [20]. Kemp's model assumes that all yarns have constant cross-sections, shaped as rectangles with semi-circular corners.

The structure of the unit cell is described by the following main parameters (Fig. 2): w_{1p} and H_{1p} are the width and height of the cross-section for the single warp yarn (Fig. 2b); w_{2p} and H_{2p} are the width and height for the double warp yarn (Fig. 2b); w_{wf} and H_{wf} are the width and height of the cross-section for the single weft yarn (Fig. 2a); H_{wp} is the height of the cross-section for the binder yarn (Fig. 2a); R_{wp} is the width of the binder yarn (Fig. 2a); φ_{wf} is the crimp angle of the weft centerline path undulating around the binder yarn (Fig. 2b); T_{w1} and T_{2p} are the distance (thickness of the adhesive layer) between the warp/weft yarns and between the double warp yarns (Fig. 2b); R_{1p} is the distance between the centerlines of single warp yarns in the top row.

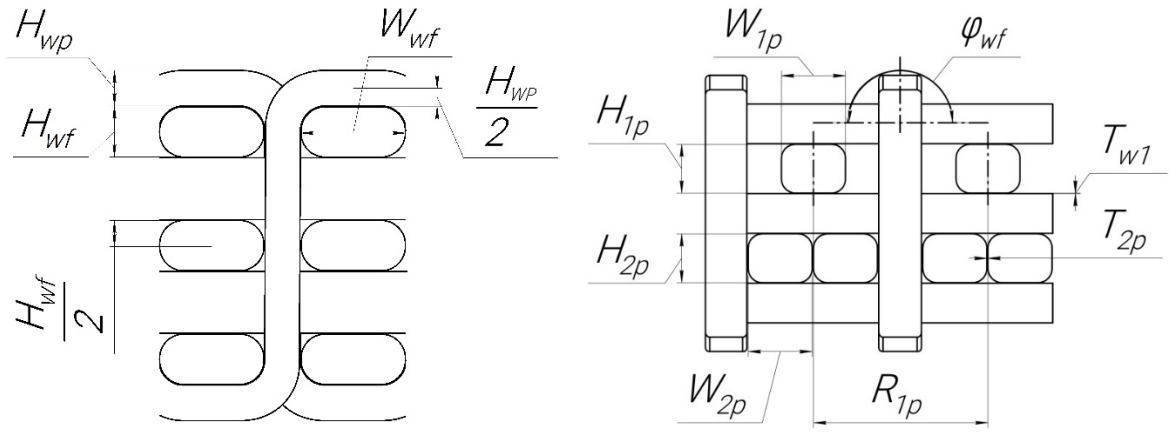

a b

Fig. 2. Kemp's racetrack model for 3DRC unit cell: cross-section of weft yarns (a) and cross-section of warp yarns (b)

The list of parameters used in this paper to describe the unit cell largely corresponds to Kemp's model; the difference is that the paths of the weft yarns are not straight in the model used but are described instead by segments and arcs of the circles around the binder yarns. The problem complexity was increased based on the results of microstructural studies.

The parameter values of the unit cell were found from the results of tomographic and microscopic studies on the composite structure.

3. Tomographic and microscopic studies

Specimens for microstructural studies of 3DRC were cut from a single plate preform together with specimens for subsequent mechanical tests. Four 15×25 mm and 25×25 mm specimens without additional surface treatments were prepared for tomographic studies (Fig. 3). Four 25×25 mm specimen slices with polished surfaces were prepared in accordance with GOST 2789 for optical microscopy studies.

Fig. 3. 3DRC specimens

Tomographic studies were carried out with a prototype microfocus X-ray computer tomograph we constructed at Saint Petersburg Electrotechnical University "LETI" [21–23]. The microfocus source was a sealed tube with an anode voltage of 130 kV, an anode current of 200 μA, and the size of the focal spot ranging from 20 μm to 100 μm. A PRODIS.Mark flat panel detector with a pixel size of 50 μm and an active area of 120x240 mm was used for recording the projection data. Combining this equipment in a laboratory tomography allows obtaining projection data with a magnification up to ×100. Preliminary studies at the laboratory setup were conducted for 25×25 mm specimens of layered and 3D reinforced carbon fibers; we detected pores with the dimensions of 10-12 μm and the parameters of the unit cells in the interlock filler (thickness and crimp angles of the yarns, adhesive layers between the yarns in the cell with the dimensions of about 15 μm).

The tomographic images were reconstructed from the results of multi-angle X-ray imaging of the specimens with the MicroCT Bruker software [24]. Figure 4 shows an example of reconstructed 3D images for structure fragments of the given 3DRC specimens.

We considered a total of 4 3D tomographic images for 4 specimens and 48 planar sections for each specimen.

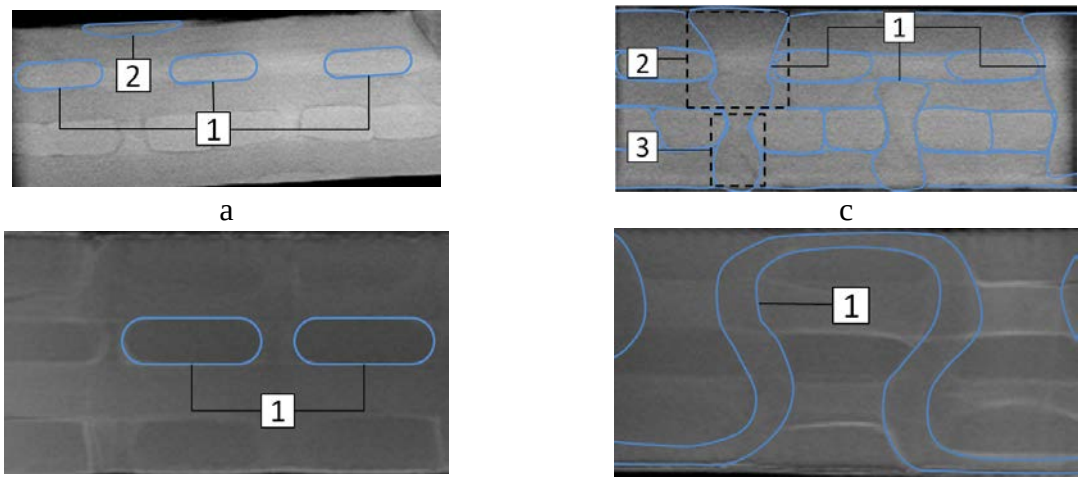

Fig. 4. Plane sections of reconstructed 3D images for structure fragments of the 3DRC specimens: (a) cross-sectional view of warp yarns (along the weft yarns); (b) cross-sectional view of weft yarns (along the warp yarns); (c) cross-sectional view of binder yarns at crossover point, (d) view along the binder yarns

Figure 2 shows an example of plane sections for reconstructed 3D images for single specimens. Analyzing all planar sections of the 3DRC specimens, we found that the paths of the warp yarns can be assumed to be straight, and the weft yarns undulating over the binder yarns deviate slightly from the straight lines described by the angle φ_{wf} (see Fig. 2 and Fig. 6), while the path of the binder yarn is S-shaped (Fig. 2d).

The cross-section of the warp and weft yarns can be described by an ellipse or a rectangle with rounded corners (Fig. 4a-1 and Fig. 4b-1). The cross-sectional shapes and areas of these yarns only vary insignificantly for all the images considered. We decided to describe the section of the warp and weft yarns with a rectangle with rounded corners, which corresponds to Kemp's model, serving as a basis for selecting the parameters of the structure to be determined. The cross-section of the binder yarn between the warp yarns has a shape close to a truncated ellipse with pointed ends (Fig. 4a-2). The cross-sectional area of the binder yarn increases in the area of contact with the warp yarns of the top row (Fig. 4c-2) and decreases in the area of contact with the warp yarns of the bottom row (Fig. 4c-3). An algorithm for modeling the unit cell in 3DRC was developed to account for this phenomenon, allowing to set the variation in the area of the binder yarn along its path.

The results of the tomographic study indicate that Kemp's model with its main assumptions (the warp and weft yarns are straight, the binder yarn is approximated with a truncated ellipse, cross-section of the yarns is described by a rectangle with rounded corners) can be taken as the basis for determining the geometric structure of 3DRC. In this case, the S-shape of the path and the variation in the cross-sectional area of the binder yarns should be additionally taken into account. The numerical values of the parameters for describing and subsequently modeling the given geometric structure of the material were found through microsection analysis.

The computed volumes of geometric objects in tomographic images of the microstructure were used to extract an estimate for the total volume fraction of the reinforcement cage, amounting to 65.51%, and estimates for the volume fractions of the warp,

weft, and binder yarns, amounting to 32.83%, 59.21%, and 7.96%, respectively; all estimates were obtained for a cell in 3DRC (Table 1).

The final stage of tomographic studies consisted of selecting orthogonal planes of the specimen slices to subsequently prepare microsections. This allowed obtaining microsections with planes of characteristic cross-sections: across the weft yarns, across the warp yarns, and across the binder yarn. Several characteristic cross-sections were obtained at different points of the yarn paths perpendicular to the plane of the section, allowing us to estimate the variation in the parameters of the cell along the path of this yarn.

Table 1. The volume fraction of yarns in the reinforcement cage of the 3DRC tested

Estimation method	V_{fo},(%)	V_{fu},(%)	V_{fp},(%)	V_{fk},(%)
Tomography	32.83	59.21	7.96	65.5
TexGen model	38.32	48.07	13.61	52.8
Simplified model of 3DRC cell (model 1)	33.86	52.95	13.19	53.9
Refined model of 3DRC cell (model 2)	33.88	58.06	8.06	68.6

Microscopic studies of 3DRC specimen microsections were carried out with a Carl Zeiss Axiovert 40 MAT microscope. About 90 micrographs with a magnification up to ×10-100 were taken in the course of microscopic studies; Figure 5 shows characteristic micrographs.

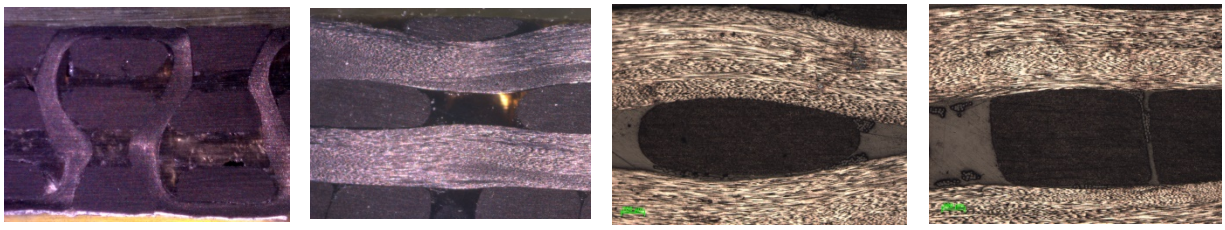

a b c d

Fig. 5. Micrographs of unit cell in 3DRC: along the binder yarns (a); along the weft yarns (b); cross-section of a single warp yarn (c); cross-section of a double warp yarn (d)

The parameter values of the 3DRC unit cell were determined from analysis of the microsections (Fig. 2): W_{1p}, H_{1p}, W_{2p}, H_{2p}, W_{wf}, H_{wf}, R_{wf}, R_{1p}, T_{w1}, T_{2p}, φ_{wf}. The study comprised 5 to 33 measurements of these parameters. The measurement data were statistically processed to obtain the mean value, the standard deviation, and the variation coefficient for each parameter (see Table 2).

Figure 6 shows example schemes for determining these parameters in four microsections of different orthogonal planes for the same specimen. Figure 6a shows the parameters of the cross-sectional areas S_{1f} and S_{wp} for the weft yarn and the stitching yarn (the latter was approximated by a truncated ellipse with pointed ends), the crimp angle φ_{wf} of the weft yarn, the heights H_{1p}, H_{2p} and the widths W_{1p}, W_{2p} for single and double warp yarns. Figure 6b shows the height H_{wf}, the width W_{wf}, the area S_{wf} and the distance R_{wf} between the centerlines of the weft yarns. Notably, the corner radii of the rectangles describing the cross-sections of the warp and weft yarns were taken equal to half the height of the respective cross-sections, and the width was defined as the greatest distance between the centers of the rounded corners. Figure 6c shows the distance R_{1p} between the centers of single warp yarns.

Figure 6d shows the thicknesses T_{w1} of the adhesive layers between the weft and warp yarns and T_{2p} between the double warp yarns.

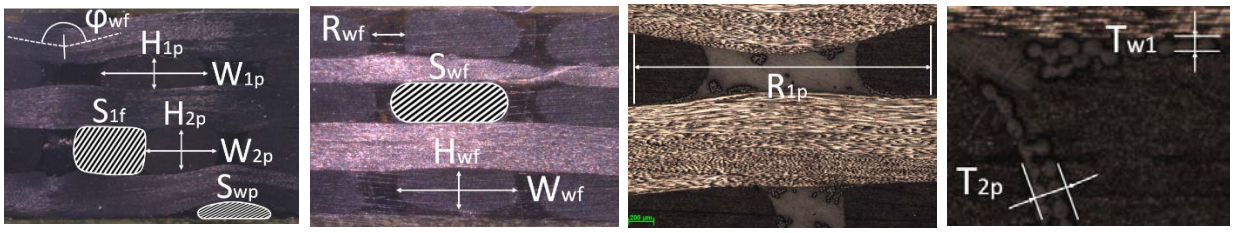

a b c d

Fig. 6. Images of 3DRC microsections with the given parameters of the braided structure: parameters 2-4, 8-12 from Table 2 (a); parameters 1, 5-7 from Table 2 (b); parameter 8 from Table 2 (c); parameters 13, 14 from Table 2 (d)

Table 2. Geometric parameters of 3DRC structure

№	Parameter	Minimum value	Maximum value	Mean value	Variation coefficient, %	Number of measurements
1	Cross-sectional area of weft yarn S_{wf}, mm^2	1.32	1.49	1.415	3.236	15
2	Cross-sectional area of warp yarn S_{1f}, mm^2	0.95	1.07	1.001	3.113	16
3	Cross-sectional area of binder yarn S_{wp}, mm^2	0.32	0.38	0.356	6.256	7
4	Crimp angle of weft yarn φ_{wf}, ^{o}	158.59	163.13	160.438	1.026	8
5	Height of weft yarn H_{wf}, mm	0.62	0.83	0.735	7.436	33
6	Width of weft yarn W_{wf}, mm	1.98	2.36	2.12	5.011	15
7	Distance between weft yarns R_{wf}, mm	0.26	0.65	0.543	10.219	16
8	Distance between centerlines of warp yarns R_{1p}, mm	3.27	3.33	3.3	0.91	5
9	Height of single warp yarn H_{1p}, mm	0.58	0.73	0.651	8.33	7
10	Width of single warp yarn W_{1p}, mm	1.55	2.01	1.825	10.69	5
11	Height of double warp yarn H_{2p}, mm	0.75	0.86	0.791	3.55	19
12	Width of double warp yarn W_{2p}, mm	1.27	1.44	1.345	4.306	12
13	Thickness of adhesive between warp and weft T_{w1}, μm	4.5	18.02	10.51	37.3	12
14	Thickness of adhesive between double warp yarns T_{2p}, μm	12.61	47.75	28.14	48.26	11

Analyzing the microsections, we detected numerous compactions of the binder yarns in the 3DRC structure considered, as illustrated by Fig. 5a. Therefore, in contrast to the assumptions formulated by Kemp [19], we assumed in the simulation that the area and cross-sectional shape of binder yarn were variable along its path. The areas S_{wf} of the binder yarn were determined at seven points along its path; the area here varied in the range from 0.32 mm^2 to 0.38 mm^2.

Considering all of the microsections obtained, we can see that a binding layer (polymer matrix) is found between the yarns of the reinforcement in the composite material considered. Thus, the subsequent statement of the micromechanics problem does not need to account for the contact interaction of reinforcing yarns without a binding layer to compute the structural stress and strain fields or predict the effective elastic characteristics of 3DRC. The parameters of the binding layer between the weft and warp yarns and between the double warp yarns, T_{w1} and T_{2p}, respectively, are given in Table 2.

The parameter values of the 3DRC structure considered were used to construct a geometric model of the unit cell for subsequent prediction of the effective elastic characteristics of the composite.

4. Modeling of the composite material structure

Computer simulation of the composite's unit cell was carried out using TexGen [3-5] and a program written based on the algorithm we developed. Using TexGen with an incomplete set of parameters from Table 1 allows us to quickly construct a geometric model of the unit cell. The unit cell was modeled using the mean values of height, width, and cross-sectional area of the yarns, the distance between the yarn centerlines, and the thickness of the bonding agent between the yarns (Table 1). The geometric model of the 3DRC cell constructed in TexGen is shown in Fig. 7a.

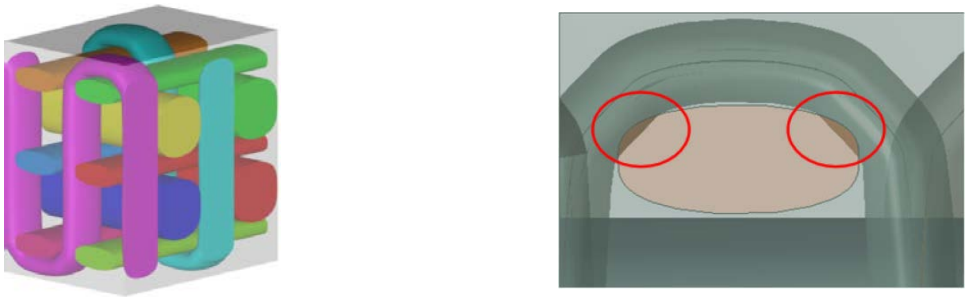

a b

Fig. 7. Model of unit cell in TexGen (a) with intersecting yarns (b)

The volume fractions of warp, weft, and stitching yarns in the 3DRC cell were computed for the model built in TexGen by the formulas from [25] (Table 1). Comparing the estimates obtained from the analysis of the tomographic images (Table 1), we found a difference of 4.44% for volume fractions of warp yarns, 9.99% for weft yarns, and 5.55% for binder yarns. In general, the difference in the volume fractions of the reinforcement cage in the cell, obtained from the results of tomographic analysis and constructed in TexGen, amounted to about 15.8% (Table 1).

The reason for this difference lies in yarn intersection errors generated at crossover points for the unit cell simulated by TexGen with the given parameters of the composite structure (Table 2). Figure 7b shows an example of intersecting weft and warp volumes in the model of the unit cell constructed in TexGen. Intersection correction is done in TexGen by removing crossovers for yarns of the same class, accordingly changing the volume fractions of these yarns in the cell. This circumstance should undoubtedly produce a

difference in the elastic characteristics of the composite predicted using the constructed geometric model of the cell.

The steps necessary for simulating 3D braiding in the cell corresponding to the experimental data include, aside from correctly describing the yarn interlocking, accounting for the variation in their cross-sectional shape along the path. For this purpose, we developed a specialized algorithm for modeling yarns in 3DRC unit cells [26]. We used the boundary-representation method (B-rep) for geometric forms of spatial structures [27-29] so that the yarns were described by surfaces and characterized by two functions, their centerline path and the cross-sectional area of the yarn along the path.

The centerline paths were simulated by straight lines for warp yarns, by line segments connected by arcs at points of crossover with binder yarns for weft yarns, and by S-shaped curves described by a segment with two arcs for binder yarns. The cross-sections of the warp and weft yarns were assumed to be constant and described by rectangles with rounded corners (the parameters are given in Table 2). The cross-section of the binder yarn was generally assumed to be variable and approximated by an ellipse with variable parameters of the semi-axes x_a, x_b.

We constructed two models of the 3DRC cell with different descriptions of the variation in the cross-section of the binder yarn. According to the first, simplified model, the cross-section was assumed to be constant, described by a rectangle with rounded corners, 0.45 mm high, 0.7 mm wide, with a corner radius of 0.1 mm and an area of 0.312 mm^2.

According to the second, refined model, the cross-sectional shape of the binder yarn varied along the trajectory, while the area remained constant, equal to S_{wp} = 0.356 mm^2, corresponding to the mean value measured in the microsections. The cross-section of the binder yarn was described by an ellipse with the parameters of the semi-axes x_a, x_b, whose values were given at seven characteristic points of the path (see Fig. 8). Point 1 corresponds to the region where the binder yarn contacts the weft yarn from the top row, points 2-6 are located in its S-shaped segment of the path with different cross-sectional values, point 7 corresponds to the region where the binder yarn contacts the weft yarn from the bottom row. The value of the semi-axis x_a of the elliptical yarn cross-section varied in the range from 0.31 mm to 0.38 mm, and the values of the semi-axis x_b from 0.28 mm to 0.62 mm. Notably, varying the cross-sectional shape along the path can lead to some variations in the anisotropy parameters for this model of the material, which was established by producing predictions for its effective elastic properties.

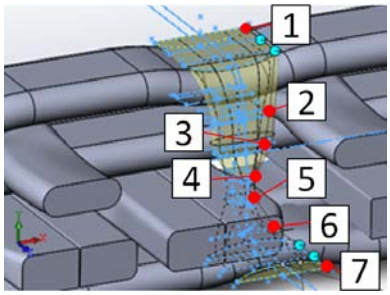

Fig. 8. Scheme for simulating the binder yarn in the 3DRC cell (model 2) with characteristic points along its path

A nonlinear approximation was adopted between the points with the given parameter values of the elliptical semi-axes characterizing the yarn cross-section, making it possible to generate smooth surfaces describing the binder yarns in the simulated cell. The parameter values of the warp and weft yarns used to construct the model of the unit cell are given in Table 2.

The developed algorithm allows describing the configuration of the binder and weft yarns in the 3DRC cell with better accuracy, accounting for the manufacturing tolerance of the reinforcement cage parameters. The geometric models of the 3DRC cell constructed by the developed algorithm and the shape of the binder yarn in the models are shown in Fig. 9. Comparing the volume fractions of different yarn sets in the constructed models of the 3DRC cell (Table 1) with tomographic estimates, we established that the difference in describing the volume fraction for model 1 amounts to 1.04% for warp yarns, to 6.26% for weft yarns, and to 5.23% for binder yarns. For model 2, these differences amount to 1.04%, 1.15%, and 0.1%, respectively. The overall difference in the volume fraction of the reinforcement cage from the tomographic data is of the order of 11.6% and 3.1% for the simplified and refined models, respectively. Apparently, the refined model of the 3DRC cell, constructed by the developed algorithm, is in agreement with the tomographic model with respect to the volume fractions of yarn sets in the reinforcement cage of the material. We should note that a larger number of finite elements are required to subsequently construct the numerical model of the refined 3DRC cell for describing the paths and shapes of the binder and weft yarns, compared to the model constructed in TexGen.

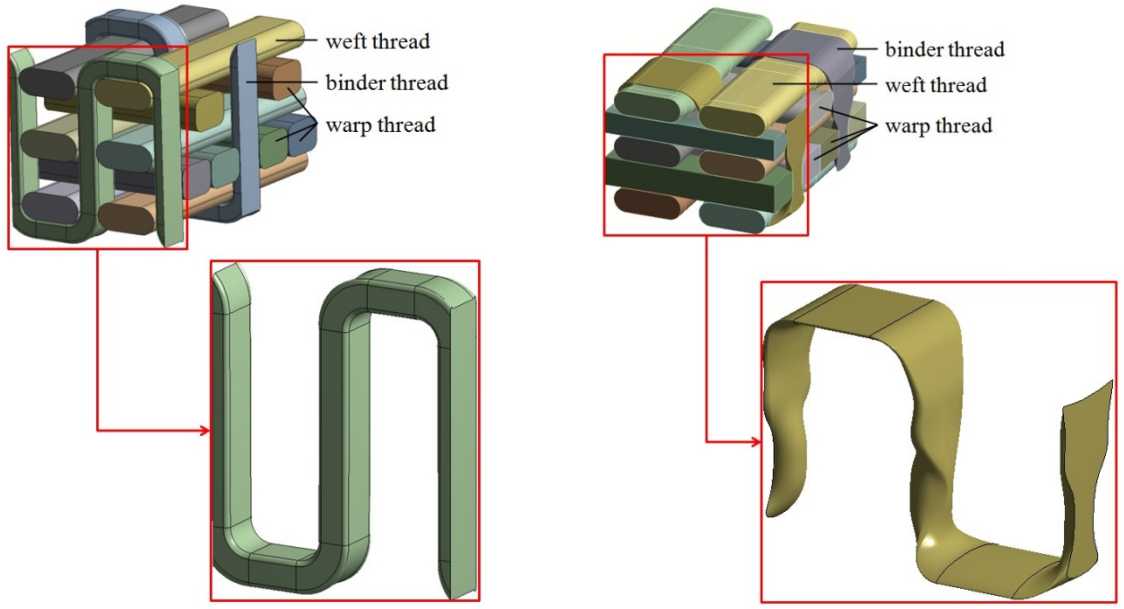

Fig. 9. Model 1 (a) and model 2 (b) of 3DRC unit cells, constructed by the algorithm developed

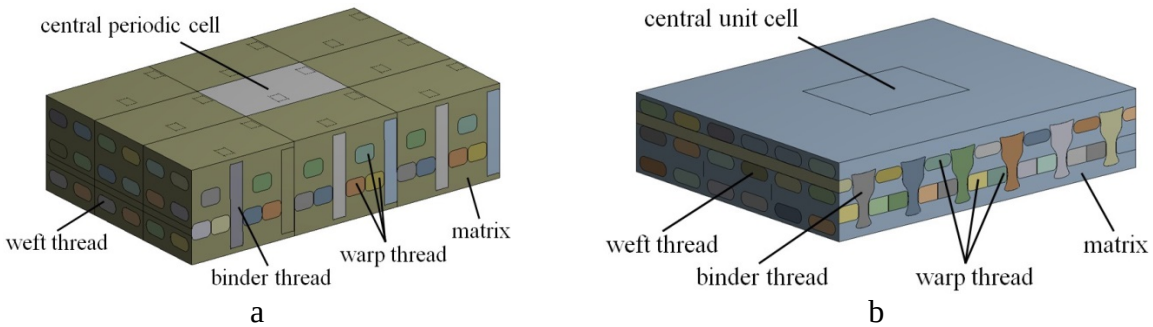

Fig. 10. Simplified model 1 (a) and refined model 2 (b) for a fragment of 3DRC

Fragments of the composite material were constructed based on geometric models of cells using threefold plane translation, including one cell in the center and those adjacent to it

(Fig. 10). A boundary-value problem was formulated below for these fragments to compute the stress and strain fields in the matrix and fibers of the composite material, predicting its mechanical characteristics by the local approximation method.

5. Statement of the micromechanics problem for a structure fragment and an algorithm for predicting the elastic characteristics in composite material

The method of local approximation was proposed by Sokolkin and Tashkinov in [15] and further elaborated in [17,18,30,31]. The method relies on the property of linearity, i.e., rapid attenuation of correlation functions corresponding to non-uniform stress and strain fields (obtained by solving several mechanical problems for composite materials) at a distance of two or three characteristic dimensions [17]. In view of this property, it was proposed to simulate the required stress and strain fields in the structural elements of the composite by its fragments containing one characteristic cell of the structural element in the center and one or two nearby layers of the adjacent cells. As a fragment is deformed, the layers of adjacent cells produce fields of structural stresses and strains in the central cell; these fields are close to those evolving in a composite material with many cells due to the local nature of the interaction between the structural elements. The values of the structural stress and strain fields averaged over the central cell of the fragment corresponding to the macroscopic stresses and strains of equivalent fields evolving in a homogeneous medium with effective mechanical properties. Consequently, solving a number of boundary-value problems for the selected composite fragment, the effective elastic properties of the composite material can be computed from the values found for the averaged (macroscopic) stresses and strains.

The local approximation method was used in [17,18,30,31] for predicting the effective elastic characteristics and solving problems of nonlinear deformation and structural failure in unidirectional fiber composites. Solving these nonlinear problems allows determining the parameters in the constitutive equations of nonlinear deformation and the strength criteria of fiber composites under arbitrary three-dimensional loading.

We considered a structural fragment of the composite including nine unit cells constructed by the developed algorithm with the mean values of the structure parameters given in Table 2. However, the local approximation method also allows solving stochastic micromechanical problems in implementations for samples of composite fragments with an arbitrary arrangement of elements [17]. We intend to explore this topic in our future studies.

Let us formulate a boundary-value problem for the 3DRC fragment. Solving it by the local approximation method, we can obtain microstress and microstrain fields in the structural elements of the composite material (matrix in the fibers) corresponding to the given macroscopic stresses or strains.

The computational scheme of the problem includes the given 3DRC fragment (Fig. 10) containing nine unit cells. According to the local approximation method, such forces $\vec{f}$ or displacements $\vec{u}$ were given at the boundary of the fragment that the strains or stresses averaged over the central cell of the fragment were equal to the given microscopic stresses σ_{ij}^{*} or strains ε_{ij}^{*}.

The system of equations for the boundary-value problem from anisotropic elasticity theory for a fragment of inhomogeneous structure includes the equilibrium equations, the Cauchy geometric relations, and the constitutive equations.

$$\sigma_{ij,j}(\vec{r}) = 0;\ \varepsilon_{ij}(\vec{r}) = \frac{1}{2}\left(u_{i,j}(\vec{r}) + u_{j,i}(\vec{r})\right);\ \sigma_{ij}(\vec{r}) = C_{ijkl}(\vec{r})\varepsilon_{ij}(\vec{r}); \tag{1}$$

$$C_{ijkl} = C_{ijkl}^{(1)}\lambda^{(1)}(\vec{r}) + C_{ijkl}^{(2)}\lambda^{(2)}(\vec{r}); \tag{2}$$

$$\lambda^{(i)}(\vec{r}) = \begin{cases} 1, (\vec{r}) \in V_p^{(i)}, \\ 0, (\vec{r}) \notin V_p^{(i)}. \end{cases}$$

Here $\sigma(\vec{r})$ and $\varepsilon(\vec{r})$ are the stress and strain tensors in the structural elements of the composite material (matrix and fibers), $C_{ijkl}^{(1)}$ and $C_{ijkl}^{(2)}$ are the elastic moduli tensors of fibers and matrix, respectively, $\lambda^{(i)}(\vec{r})$ is the indicator function, where *i* is an index corresponding to the structural element (1 corresponds to the fiber, 2 to the matrix).

System (1) and (2) is closed by boundary conditions and conditions for adjusting them by local approximation [17,18,30,31]. Displacements $\vec{u}$ or forces $\vec{f}$ are given at the fragment boundary Γ; they are computed in terms of auxiliary tensors for adjusting the boundary conditions A_{ijkl} or B_{ijkl} and the given microscopic stresses σ_{ij}^* or strains ε_{ij}^*:

$$\hat{\sigma}_{ij}(\vec{r}) n_j(\vec{r}) = f_i\big|_{r\in\Gamma}, \quad \hat{\varepsilon}_{ij} r_j = u_i^0; \tag{3}$$

$$\hat{\sigma} = A_{ijkl}\sigma_{ij}^*, \; \hat{\varepsilon} = B_{ijkl}\varepsilon_{ij}^*. \tag{4}$$

The boundary conditions (3) and (4) allow obtaining the structural stress and strain fields from the solution of the boundary problem in the central cell of the fragment, corresponding to the given macroscopic stresses or strains. For this purpose, we should first determine the components of the tensors for adjusting the boundary conditions A_{ijkl} or B_{ijkl} from the solution of six test problems on the deformation of the fragment considered. However, conditions (4) do not have to be satisfied precisely to predict the effective elastic properties of the composite. Here it is sufficient to solve six boundary problems for the fragment under arbitrary conditions (3) independent of each other and obtain the stresses σ_{ij}^* and strains ε_{ij}^* by averaging with respect to the central cell:

$$\sigma_{ij}^* = \frac{1}{V_l}\int_{V_l} \sigma_{ij} dV, \; \varepsilon_{ij}^* = \frac{1}{V_l}\int_{V_l} \varepsilon_{ij} dV. \tag{5}$$

We can obtain systems of linear equations by assuming these averaged stresses to be macroscopic, arising in an equivalent homogeneous medium, and substituting them for all k problems (k =1,2,…,6) into Hooke's law for an anisotropic medium in matrix form [32] with the matrix of effective stiffnesses C_{ij}^* or compliances S_{ij}^*.

$$\sigma_i^k = C_{ij}^* \varepsilon_j^k, \; \varepsilon_i^k = S_{ij}^* \sigma_j^k. \tag{6}$$

The corresponding tensor and matrix notations for stresses, strains, and elastic moduli for writing Hooke's law are given, for example, in [33]. Performing a rearrangement, we can divide systems of equations (6) into six systems of linear equations relative to the unknowns C_{ij}^* or S_{ij}^*.

$$\begin{aligned} &\sigma_1^k = C_{1j}^* \varepsilon_j^k, \; \sigma_2^k = C_{2j}^* \varepsilon_j^k, \; \sigma_3^k = C_{3j}^* \varepsilon_j^k, \; \sigma_4^k = C_{4j}^* \varepsilon_j^k, \; \sigma_5^k = C_{5j}^* \varepsilon_j^k, \; \sigma_6^k = C_{6j}^* \varepsilon_j^k; \\ &\varepsilon_1^k = S_{1j}^* \sigma_j^k, \; \varepsilon_2^k = S_{2j}^* \sigma_j^k, \; \varepsilon_3^k = S_{3j}^* \sigma_j^k, \; \varepsilon_4^k = S_{4j}^* \sigma_j^k, \; \varepsilon_5^k = S_{5j}^* \sigma_j^k, \; \varepsilon_6^k = S_{6j}^* \sigma_j^k. \end{aligned} \tag{7}$$

Solving these systems (7) with respect to the unknowns C_{ij}^*, S_{ij}^*, we can determine the effective stiffnesses, compliance, and technical elastic constants for an anisotropic homogeneous medium equivalent to 3DRC.

Considering the boundary-value problems (k =1,2,…,6) mentioned above, it is the most convenient to choose the problems on uniaxial strain in the fragment along each of the coordinate axes and pure shear in three coordinate planes. The corresponding boundary conditions were given by the displacements, and one central point of the fragment was additionally fixed to achieve the stability of numerical simulations performed to solve FEM

problems. Our computations of effective stiffnesses C_{ij}^* and compliances S_{ij}^* from the solution of system (7) assumed that the material was orthotropic and the elastic moduli tensor satisfied the symmetry conditions. For this reason, the diagonal components C_{ij}^*, S_{ij}^*, reflecting the mutual influence of shear strains on each other and on longitudinal stresses, were taken equal to zero, while the components of the effective compliance matrix S_{ij}^* $(i, j = 1,2,3)$, located symmetrically relative to the main diagonal, were averaged for subsequent computations of elastic constants.

The given composite model assumed that the yarns impregnated with a polymer adhesive consisted of a unidirectionally reinforced transversely isotropic composite material whose elastic properties were computed by the Chamis ratios [34]. The elastic properties of impregnated carbon filament and polymer matrix used in the computations are given in Table 3.

Table 3. Properties of structural elements in 3DRC

Material	E_x, GPa	E_y, GPa	E_z, GPa	ν_{xy}	ν_{yz}	ν_{xz}	G_{xy}, GPa	G_{yz}, GPa	G_{xz}, GPa
Impregnated carbon filament	200	9.5	9.5	0.014	0.24	0.014	6.93	12.84	6.93
Polymer matrix	3.7			0.38			1.34		

The boundary-value problem formulated in accordance with the local approximation method for the composite fragment was solved numerically by the finite element method (FEM) using the ANSYS software. Discretization of the fragments was performed using *SOLID*186 solid-state elements. The computational mesh comprised 2.7 million elements and 5.8 million nodes, selected by estimating the convergence of the numerical solution on the predicted values of the elastic moduli (the difference was no more than 1%).

6. Discussion of computational results and comparison with experimental data

We numerically solved six boundary problems on tension along the coordinate axes and with a shift in the coordinate planes of the model fragments constructed for the simplified and refined 3DRC structures, obtaining fields of structural stresses and strains in the central cell of the fragments. Averaging these fields over the volume of the central cell yielded the corresponding values of macrostresses and macrostrains for a homogeneous medium with effective properties; next, the above-described algorithm was applied to produce the effective compliances and elastic constants for 3DRC.

Table 4 and Figure 11 show a complete set of effective elastic characteristics, computed by two 3DRC models, simplified (model 1) and refined (model 2). For comparison, Table 4 presents the experimental estimates of the effective elastic moduli E_x, E_y, G_{xy} (the OX axis is directed along the warp yarns, the OY axis along the weft yarns), obtained by the material's manufacturer. Mechanical tests were performed for the same 3DRC specimens that participated in microstructural studies. Uniaxial tensile tests were performed by the ASTM D3039 standard with a loading rate of 1 mm/min for two sets of strip specimens, the variation coefficient for the mean values of Young's modulus amounted to 2.6%. Shear tests were performed by the ASTM D5379 standard for a set of five V-notched specimens at a loading rate of 2 mm/min, the variation coefficient for the mean values of the shear modulus amounted to 12.3%. For convenience, Table 4 additionally shows experimental and model values for the volume fractions of reinforcing fibers in 3DRC cells: the total value (υ_f) and

the values corresponding to the directions of the OX and OY axes $(\upsilon_{fx}, \upsilon_{fy})$. Furthermore, Table 4 shows the relative differences between δ^1 and δ^2 (%) for the experimental values of elastic characteristics and volume fractions of fibers (x^e) and those computed by the first (x^{m1}) and the second (x^{m2}) model.

$$\delta^i = \frac{(x^e - x^{mi})}{x^e} * 100 . \quad (8)$$

Table 4. Computational and experimental effective elastic properties and volume fractions of reinforcing fibers in 3DRC

Characteristics of 3DRC	Computation		Experiment	δ^1, %	δ^2, %
	Model 1	Model 2			
E_x, GPa	46.18	49.43	52.38	11.84	5.63
E_y, GPa	61.54	76.29	71.35	13.74	-6.93
E_z, GPa	11.59	8.67			
ν_{xy}	0.02	0.02			
ν_{yz}	0.26	0.28			
ν_{xz}	0.29	0.31			
G_{xy}, GPa	6.87	8.33	7.92	13.24	-5.20
G_{yz}, GPa	6.20	7.62			
G_{xz}, GPa	6.56	7.43			
υ_{fx}, %	33.86	33.88	32.83	-3.14	-3.20
υ_{fy}, %	52.95	58.06	59.21	10.57	1.94
υ_f, %	53.90	68.60	65.5	17.71	-4.73

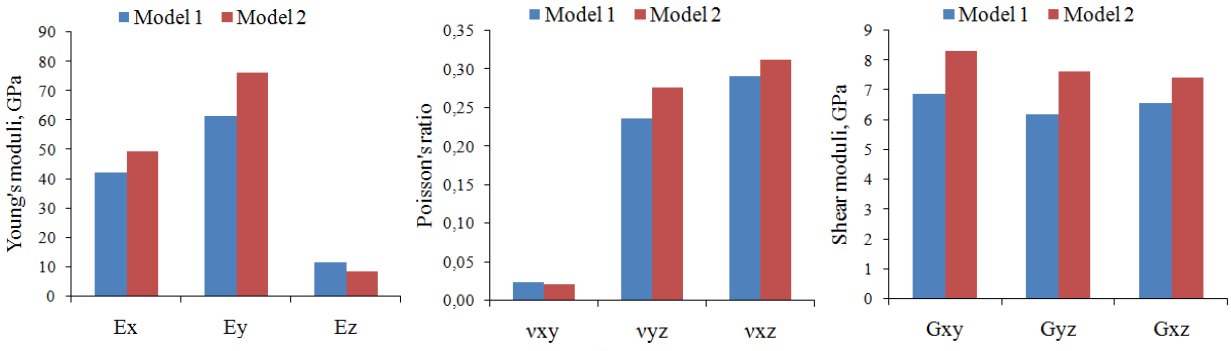

a b c

Fig. 11. Comparison of effective Young's moduli (a), Poisson's ratios (b), and shear moduli (c) computed for the first (simplified) and second (refined) 3DRC models

Analyzing the results obtained (see Table 4), we found that the refined geometric model of the unit cell, along with the technique for solving boundary-value problems for the fragment of the 3DRC structure with subsequent averaging of the obtained stress fields with respect to the central cell of the fragment, allows predicting the effective elastic properties of 3D reinforced composite materials with good accuracy ($\delta \approx$ 5.2-6.5 %). Using a simplified model of the unit cell produces large differences ($\delta \approx$ 11.8-13.7%) in the computational and

experimental data, which is primarily due to the difference in the volume fractions of the weft and binder yarns in the simplified model from the experimental values.

We should note (see Table 4) that the volume fractions of fibers v_{fx} close to the experimental values ($\delta \approx 3\%$) were obtained for the weft for both 3DRC models. At the same time, the prediction accuracy of effective Young's modulus E_x differs by two times for the two models. Therefore, to achieve good prediction accuracy for effective Young's modulus for the weft ($\delta \approx$ 5-6%), not only good agreement with the experimental volume fractions of fibers in this direction but also agreement with the total volume fraction of fibers for the cell as a whole should be obtained in the geometric model of 3DRC, which is provided by the refined model of the cell (model 2).

Interestingly, the prediction errors of the elastic moduli along the OX and OY axes have different signs in the refined model of the composite. The anisotropy parameter of the material E_x / E_y, equal to 0.648 for this model, differs more from the experimental value $E_x / E_y = 0.73$ than for the simplified model, where $E_x / E_y = 0.75$. The ratio of the volume fractions of fibers in these directions (v_{fx} / v_{fy}) is closer to the experimental value (0.554) for the refined model $(v_{fx} / v_{fy} = 0.583)$ than for the simplified model $(v_{fx} / v_{fy} = 0.639)$. The likely reason for this is the variation in the cross-sectional shape of the binder yarn along its path in the refined model of the 3DRC cell. Moreover, we can see that the greatest error in predicting the elastic modulus ($\delta \approx 7\%$) is observed in the refined model for the weft fibers E_y whose volume fraction v_{fy} is described with good accuracy ($\delta \approx 2\%$).

The difference between the computational and experimental values can also be explained by the difference in the values of the elastic characteristics of complex warp and weft yarns given by the model from the values detected in the composite, as well as by the scatter of the values of the structural parameters in the 3DRC specimen tested. Therefore, we intend to further focus on formulating and solving a stochastic mechanical problem using the developed structural model and the local approximation method to estimate the mean values, variances, and correlation coefficients of the effective elastic characteristics in 3DRC based on the scatter found for the structural parameters of the cell (see Table 2).

7. Conclusions

We have obtained the following key findings:

- microstructural studies were carried out to determine the mean values and variation coefficients for 14 main parameters of the braid unit cell in the given 3D reinforced composite.

- we have constructed an algorithm along with a new model for a braid unit cell of a composite with a modified cross-sectional shape of the binder yarn along the path with the parameters corresponding to the experimental mean values extracted.

- the model allows extracting the volume fractions for different yarn sets in the composite cell, close to experimental estimates (the difference is about 1%), providing accurate predictions for the effective elastic characteristics.

We have developed a new technique based on the local approximation for predicting the effective elastic characteristics of 3D reinforced composite materials. The technique incorporates numerical solutions to spatial boundary-value problems for 3D structural fragments of the composite with subsequent averaging of the stress and strain fields obtained with respect to the central cell of the fragment. We have constructed fragments of the 3DRC structure including nine reference unit cells with mean values of the structure's parameters. The technique presented was used to numerically solve the boundary-value problems for the

constructed structure fragments and compute a full range of effective elastic properties for the given 3DRC.

Comparison with the experimental data showed good accuracy for the proposed new model of the braid unit cell (difference of 5.2-6.5% for the predictions of effective Young's moduli and the shear modulus in the plane of the warp and weft yarns), while the model constructed via the standard TexGen software package yielded predictions with the difference of 11.8-13.7%. We can therefore assume that geometric models of 'ideal' 3DRC cells constructed via standard software without accounting for manufacturing tolerances of the structure parameters cannot provide satisfactory accuracy for the predictions of the effective elastic characteristics in the real composite.

A promising avenue to explore is the further simulation of the stochastic 3DRC structure accounting for both mean values extracted and the variation coefficients of the structural parameters characterizing the geometry of the braid unit cell. Our follow-up studies will formulate and solve a stochastic boundary-value problem for fragments of an arbitrary 3DRC structure by the local approximation method. It would be interesting to develop and implement an algorithm for selecting boundary conditions in boundary-value problems for fragments of the 3DRC structure, subsequently obtaining fields of microstructural stresses and strains in the central cell of the fragment corresponding to predefined macroscopic quantities. This will make it possible to simulate the mechanisms of structural failure (damage accumulation) in the cell, describe nonlinear deformation and assess macroscopic strength under various loading conditions of the composite material.

References

1. Carey JP. *Handbook of Advances in Braided Composite Materials: Theory, Production, Testing and Applications*. Woodhead Publishing; 2016.
2. Bogomolov PI, Kozlov IA, Birulya MA. Review of modern technologies for manufacturing volume-reinforcing preforms for promising composite materials. *Technical and technological problems of the service*. 2017;1(39): 22-27.
3. Brown LP, Long AC, Jones IA. Recent developments in the realistic geometric modelling of textile structures using TexGen. In: *Materials 1st International Conference on Digital Technologies for the Textile Industries*. Manchester; 2013. p.12.
4. Long AC, Brown LP. Modelling the geometry of textile reinforcements for composites: TexGen. In: *Composite Reinforcements for Optimum Performance*. Woodhead Publishing; 2011. p.239-264.
5. Long AC. *Design and manufacture of textile composites*. Woodhead Publishing; 2005.
6. Espadas-Escalante JJ, van Dijk NP, Isaksson P. The effect of free-edges and layer shifting on intralaminar and interlaminar stresses in woven composites. *Compos. Struct.* 2018;185: 212-220.
7. Lomov SV, Gusakov AV, Huysmans G, Prodromou A, Verpoest I. Textile geometry preprocessor for meso-mechanical models of woven composites. *Compos Sci Technol.* 2000;60(11):2083-2095.
8. Verpoest I, Lomov SV. Virtual textile composites software WiseTex: Integration with micro-mechanical, permeability and structural analysis. *Compos Sci Technol.* 2005;65(15-16): 2563-2574.
9. Lomov S, Perie G, Ivanov D, Verpoest I, Marsal D. Modeling three-dimensional fabrics and three-dimensional reinforced composites: Challenges and solutions. *Text Res J.* 2011;81(1): 28-41.
10. Li M, Wang P, Boussu F, Soulat D. Investigation of the Strength Loss of HMWPE Yarns During Manufacturing Process of 3D Warp Interlock Fabrics. *Applied Composite Materials.* 2022;29: 357–371.

11. *Techtext CAD*. URL: https://www.tensiontech.com/software/techtext-cad (access date 10.11.2021).
12. Zeng X, Li Y, Ruan D, Koehl, L. (Eds.). *Computational Textile. Studies in Computational Intelligence*. 2007.
13. Hearle JWS. The challenge of changing from empirical craft to engineering design. *Int J Cloth Sci Technol*. 2004;16(1-2): 141-152.
14. Hobbs RE, Ridge IML. A new estimate of the yarn-on-yarn friction coefficient. *Journal of Strain Analysis for Engineering Design*. 2018;53(4): 191-196.
15. Sokolkin YV, Tashkinov AA. *Mechanics of deformation and destruction of structurally inhomogeneous bodies*. 1984.
16. Evdokimov AA, Gulyaev IN, Nacharkina AV. Investigation of the physicomechanical properties of volume-reinforced carbon fiber reinforced plastic. *Trudy VIAM.* 2020;3(87): 66-73.
17. Anoshkin AN, Sokolkin YV, Tashkinov AA. Microstress fields and the mechanical properties of disordered fiber composites. *Mech Compos Mater.* 1991;26(5): 628-633.
18. Tashkinov AA, Anoshkin AN. Predicting the transverse strength of unidirectional composites under combination loading. *Mech Compos Mater.* 1996;31(4): 346-351.
19. Kemp A. An Extension of Peirce's Cloth Geometry to the Treatment of Non-circular Threads. *Journal of the Textile Institute Transactions.* 1958;49(1): 44-48.
20. Avanaki MJ, Jeddi AAA. Mechanical behavior of regular twill weave structures; part I: 3D meso-scale geometrical modelling. *J. Eng. Fibers Fabr.* 2015;10(1): 115-127.
21. Bessonov VB, Larionov IA, Obodovsky AV. Features of the development of software and hardware systems for microct. *Physical bases of instrumentation* 2019;8(4): 23-33. (In Russian)
22. Bessonov VB, Gryaznov AY, Larionov IA, Osokin VM, Staroverov NE, Kholopowa ED. Development of an algorithm for finding defects on tomographic slices for studying composite materials by microfocus tomography. *Physical bases of instrumentation*. 2020;9(4): 60-63. (In Russian)
23. Bessonov VB, Obodovskiy AV, Gryaznov AY, Klonov VV, Larionov IA, Osokin VM. About possibility of detecting micron-size defects in layered structures using the method of microfocus tomography. *Journal of Physics: Conference Series.* 2017;872(1): 128976.
24. *Bruker Corporation*. URL: https://www.bruker.com/ (access date 10.11.2021).
25. Ansar M, Xinwei W, Chouwei Z. Modeling strategies of 3D woven composites: A review. *Compos Struct.* 2011;93(8): 1947-1963.
26. Anoshkin AN, Pisarev PV, Ermakov DA, Merzlyakova NA. Prediction of elastic characteristics of spatially reinforced composite materials. *IOP Conference Series: Materials Science and Engineering*. 2018;406: 012023.
27. Hiemstra RR, Shepherd KM, Johnson MJ, Quan L, Hughes TJR. Towards untrimmed NURBS: CAD embedded reparameterization of trimmed B-rep geometry using frame-field guided global parameterization. *Comput Methods Appl Mech Eng.* 2020;369: 113227.
28. Maquart T, Elguedj T, Gravouil A, Rochette M. 3D B-Rep meshing for real-time data-based geometric parametric analysis. Adv Model Simul Eng Sci 2021;8(1): 8.
29. Sun Y, Lueth TC. SGCL: A B-Rep-Based Geometry Modeling Language in MATLAB for Designing 3D-Printable Medical Robots. In: *IEEE International Conference on Automation Science and Engineering*. IEEE; 2021. p. 21201930.
30. Anoshkin AN. On one approach to solving a nonlinear spatial problem of micromechanics for unidirectional fibrous composites. *Bulletin of the Perm State Technical University. Mathematical modeling of systems and processes.* 1997;5: 4-10.

31. Anoshkin AN. Micromechanical analysis of inelastic deformation of unidirectional fibrous composites under multiaxial loading and shear. Compound materials Mechanics. 2003;39(5): 575-586. (In Russian)
32. Fudzii T, Dzako M. *Fracture mechanics of compound materials.* Moscow: Mir; 1982. (In Russian)
33. Skudra AM, Bulavs FY. *Strength of reinforced plastics*. Moscow: Khimiya; 1982. (In Russian)
34. Chamis C. C. Mechanics of composite materials: past, present, and future. *J. Compos Technol Res ASTM*. 1989;11: 3-14.

THE AUTHORS

Anoshkin A.N.
e-mail: aan-02@yandex.ru
ORCID: 0000-0002-3972-9902

Pisarev P.V.
e-mail: pisarev85@live.ru
ORCID: 0000-0001-5103-4815

Ermakov D.A.
e-mail: den032895@yandex.ru
ORCID: 0000-0002-3584-1286

Roman K.V.
e-mail: kvroman@pstu.ru
ORCID: 0000-0002-4357-8932